Journal of Materials Chemistry C

PAPER

View Article Online
View Journal | View Issue

Cite this: J. Mater. Chem. C, 2016, 4, 5779

Controlling mixed conductivity in $Na_{1/2}Bi_{1/2}TiO_3$ using A-site non-stoichiometry and Nb-donor doping

Linhao Li,[a] Ming Li,[b] Huairuo Zhang,[a] Ian M. Reaney[a] and Derek C. Sinclair*[a]

Precise control of electronic and/or ionic conductivity in electroceramics is crucial to achieve the desired functional properties as well as to improve manufacturing practices. We recently reported the conventional piezoelectric material $Na_{1/2}Bi_{1/2}TiO_3$ (NBT) can be tuned into a novel oxide-ion conductor with an oxide-ion transport number (t_{ion}) > 0.9 by creating bismuth and oxygen vacancies. A small Bi-excess in the nominal starting composition ($Na_{0.50}Bi_{0.50+x}TiO_{3+3x/2}$, x = 0.01) or Nb-donor doping ($Na_{0.50}Bi_{0.50}Ti_{1-y}Nb_yO_{3+y/2}$, $0.005 \leq y \leq 0.030$) can reduce significantly the electrical conductivity to create dielectric behaviour by filling oxygen vacancies and suppressing oxide ion conduction ($t_{ion} \leq 0.10$). Here we show a further increase in the starting Bi-excess content ($0.02 \leq x \leq 0.10$) reintroduces significant levels of oxide-ion conductivity and increases $t_{ion} \sim 0.4$–0.6 to create mixed ionic/electronic behaviour. The switch from insulating to mixed conducting behaviour for $x > 0.01$ is linked to the presence of Bi-rich secondary phases and we discuss possible explanations for this effect. Mixed conducting behaviour with $t_{ion} \sim 0.5$–0.6 can also be achieved with lower levels of Nb-doping ($y \sim 0.003$) due to incomplete filling of oxygen vacancies without the presence of secondary phases. NBT can now be compositionally tailored to exhibit three types of electrical behaviour; Type I (oxide-ion conductor); Type II (mixed ionic-electronic conductor); Type III (insulator) and these results reveal an approach to fine-tune t_{ion} in NBT from near unity to zero. In addition to developing new oxide-ion and now mixed ionic/electronic NBT-based conductors, this flexibility in control of oxygen vacancies allows fine-tuning of both the dielectric/piezoelectric properties and design manufacturing practices for NBT-based multilayer piezoelectric devices.

Received 27th April 2016,
Accepted 20th May 2016

DOI: 10.1039/c6tc01719c

www.rsc.org/MaterialsC

Introduction

It has been long known that low levels of non-stoichiometry in functional oxides, either associated with intentional element doping or unintentional element loss/gain during processing or impurities in raw materials can induce significant changes in functional properties.[1–3] Understanding the defect chemistry and controlling non-stoichiometry in functional oxides is a powerful and proven approach to improve the desired electronic, ionic, mixed ionic/electronic and/or polar dielectric properties of existing materials, design new materials and optimise manufacturing practices for various modern electronic devices. In particular, the presence of low levels of oxygen vacancies can play an important role in the functional properties. Two classical examples are $BaTiO_3$-based multilayer ceramic capacitors (MLCCs) with base-metal electrodes and $Pb(Zr,Ti)O_3$ (PZT)-based piezoelectric devices.

$BaTiO_3$-based MLCCs with base-metal electrodes require sintering at low oxygen partial pressure (pO_2) to avoid oxidation of metal electrodes.[4] Such sintering conditions will lead to titanium reduction, generating undesired n-type electronic conduction. Acceptor doping with the creation of oxygen vacancies is useful to limit reduction of titanate-based materials under the reducing processing conditions. On the other hand, the level of oxygen vacancies has to be minimised to control the insulation resistance and tan δ at elevated temperatures. Elaborate elemental doping schemes in $BaTiO_3$ are required to achieve balanced oxygen vacancy concentration, which enables manufacturing of MLCCs using base-metal electrodes at low pO_2 without titanium reduction while maintaining device reliability and lifetime.

A-site non-stoichiometry linked to oxygen vacancies is not an issue in titanate-based perovskite dielectrics such as (Ba,Sr)-TiO_3 that contain only alkaline earth A-site cations but is a known issue in others such as PZT due to PbO-loss. In the processing

[a] Sir Robert Hadfield Building, Department of Materials Science & Engineering, Mappin Street, University of Sheffield, Sheffield, S1 3JD, UK. E-mail: d.c.sinclair@sheffield.ac.uk
[b] Department of Mechanical, Materials and Manufacturing Engineering, University of Nottingham, University Park, Nottingham, NG7 2RD, UK

of ceramics that contain volatile A-site species, this is often circumvented by either; (i) adding an excess of the volatile species to the starting composition; or (ii) donor-doping on the A- or B-site, *e.g.* La-doping for Pb in PZT.[4–10] In both cases, the additive and/or dopant concentration level(s) need to be well balanced to control the oxygen vacancy concentration required for the creation of pinning defects that influence domain wall motion.[10,11] This can be employed to manufacture 'hard' and 'soft' piezoelectric ceramics to tune functional properties (*e.g.*, piezoelectric constant, coercive field, depolarisation temperature, quality factor, relative permittivity and dielectric loss) to suit different applications.[10]

The ferroelectric perovskite $Na_{1/2}Bi_{1/2}TiO_3$ (NBT) is known to exhibit interesting and diverse structure-composition-property relationships.[12–21] A combination of A-site (Na, Bi) disorder, Bi- and Ti-displacements and in-phase and out-of-phase octahedral tilting ensures the crystal chemistry and polymorphism of NBT remain a challenging subject, especially below *ca.* 520 °C where distortions from the ideal 'cubic' cell are reported to occur.[13,14,22–26] The electrical conductivity of undoped NBT materials are known to be critically dependent on low levels of A-site non-stoichiometry, commonly ±0.02 from the nominally stoichiometric 0.50Na : 0.50Bi ratio.[5,27] Hiruma *et al.* were the first to show the room temperature dc resistivity of NBT ceramics based on 0.01 Bi-excess (*e.g.* 0.50Na : 0.51Bi) or 0.01 Na-deficiency (*e.g.* 0.49Na : 0.50Bi) to exceed those based on 0.01 Na-excess or 0.01 Bi-deficiency by up to three orders of magnitude.[28] Furthermore, it is widely reported that undoped and nominally A-site stoichiometric NBT ceramics can be leaky with $\tan\delta > 0.10$ at >300 °C whereas others report excellent dielectric behaviour with $\tan\delta < 0.02$ at ~600 °C.[29–31] Such significant variations in electrical behaviour from nominally similar starting compositions demonstrate the importance of controlling the loss of any Na and/or Bi-oxides as volatile species during the processing of NBT-based materials. Detecting these small variations in A-site stoichiometry is challenging for conventional analytical methods (see ESI in ref. 27 for more details) and electrical property measurements are sensitive tools to probe the composition-property relationships of NBT-based materials.

We have recently used a combination of Impedance Spectroscopy (IS), O^{18} Time-of-Flight Secondary Ion Mass Spectrometry (ToF SIMS) and oxygen concentration cell (electromotive force, EMF) measurements to show nominally Na-rich (*e.g.* $Na_{0.51}Bi_{0.50}TiO_{3.005}$) or Bi-deficient NBT (*e.g.* $Na_{0.50}Bi_{0.49}TiO_{2.985}$) ceramics and nominally stoichiometric NBT to be excellent oxide-ion conductors with oxide-ion transfer numbers (t_{ion}) exceeding ~0.9 at 600 °C whereas nominally Na-deficient (*e.g.* $Na_{0.49}Bi_{0.50}TiO_{2.995}$) or Bi-excess NBT (*e.g.* $Na_{0.50}Bi_{0.51}TiO_{3.015}$) ceramics are electrically insulating but retain $t_{ion} \sim 0.1$ at 600 °C.[5,27] This showed undoped NBT ceramics to be mixed ion-electron conducting materials where the magnitude of the bulk conductivity, σ_b, and t_{ion} are heavily dependent on the nominal Na : Bi ratio in the starting composition. We attribute the source of oxygen vacancies in nominally stoichiometric NBT to be associated with low levels of Bi_2O_3-loss during ceramic processing. The conduction properties of nominally A-site non-stoichiometric compositions rely on a deficiency of Bi_2O_3 to promote bulk oxide-ion conduction or an excess of Bi_2O_3 to compensate for Bi_2O_3-loss during processing to ensure bulk oxide-ion conduction is suppressed and dielectric behaviour is obtained.

Chemical doping with Mg for Ti (acceptor-type, *i.e.* $Ti^{4+} + O^{2-} \rightarrow Mg^{2+}$) can significantly increase the oxide-ion conductivity in NBT with t_{ion} approaching unity to promote solid electrolyte behaviour whereas Nb-doping for Ti (*i.e.* donor-type, $Ti^{4+} \rightarrow Nb^{5+} + 1/2O^{2-}$) can suppress the oxygen vacancy concentration and oxide-ion conductivity such that excellent dielectric behaviour can be obtained with $\tan\delta < 0.02$ at 600 °C.[9,27] Such behaviour is desirable for NBT-based applications, *e.g.* as Pb-free piezoelectrics and/or as a solid solution member in temperature stable, high permittivity MLCCs operating at >175 °C.

Here we report the electrical properties of NBT-based ceramics with a wider range of nominal Bi nonstoichiometry ($Na_{0.50}Bi_{0.50+x}TiO_{3+3x/2}$, $0.00 \leq x \leq 0.10$) and Nb-doping ($Na_{0.50}Bi_{0.50}Ti_{1-y}Nb_yO_{3+y/2}$, $0.000 \leq y \leq 0.100$). The solid solutions limits are low with $x < 0.01$ and $y < 0.030$ but dramatic changes in the bulk conduction mechanisms are reported. We show an apparently peculiar behaviour that, as compared to the resistive Bi-excess composition ($x = 0.01$) reported recently, a further increase of Bi content (*e.g.*, $x \geq 0.02$) reintroduces significant levels of oxide-ion conductivity and increases t_{ion} to intermediate levels of ~0.4–0.6 to create mixed ionic/electronic behaviour. This mixed conduction behaviour with $t_{ion} \sim 0.5$ is also observed in single-phase samples with low levels of Nb-doping ($y = 0.002$, 0.003). The results reveal, in addition to conducting NBT compositions with t_{ion} close to unity and insulating NBT compositions with t_{ion} close to zero shown in our previous reports, NBT compositions can now be fine-tuned to give intermediate t_{ion} values of ~0.4 to 0.6. This has important implications for the compositional control of NBT-based materials for various dielectric, piezoelectric, oxide-ion and now mixed ionic/electronic conducting applications.

Experimental

Ceramics of $Na_{0.50}Bi_{0.50+x}TiO_{3+3x/2}$ (for $x = 0.00$, 0.01, 0.02, 0.05 and 0.10) and $Na_{0.50}Bi_{0.50}Ti_{1-y}Nb_yO_{3+y/2}$ (for $y = 0.002$, 0.003, 0.030, 0.050 and 0.100) were prepared by the conventional solid state route. Na_2CO_3 (99.5%, Sigma-Aldrich), Bi_2O_3 (99.9%, Acros Organics), TiO_2 (99.9%, Sigma-Aldrich) and Nb_2O_5 powders (99.9%, Sigma-Aldrich) were used as raw materials. The powders were pre-dried (300 or 800 °C for 2 h, as appropriate) before weighing. The mixtures of raw materials were ball milled in isopropanol using yttria-stabilized zirconia milling media for 6 h, then dried at 80 °C, sieved, and calcined at 800 °C for 2 h in air. The resultant powders were then ball milled for 4 h followed by drying, sieving and a 2 h calcination at 850 °C and another 6 h ball milling. Green bodies were first formed by a uniaxial steel die and then isostatically pressed at 200 MPa. Prior to sintering at 1050–1150 °C for 2 h, pellets were covered in calcined powder of the same composition to minimise volatilisation.

The crystalline phases were determined by X-ray powder diffraction (XRD) analysis (high-resolution STOE STADI-P diffractometer, STOE & Cie GmbH, Darmstadt, Germany) using $CuK_{\alpha 1}$ radiation on sintered and crushed samples. A combination of scanning electron microscopy (SEM, JEOL 6400, JEOL Ltd, Tokyo, Japan), energy dispersive X-ray spectroscopy (EDX, Oxford Link ISIS, Oxford Instruments Ltd, Oxfordshire, UK), and transmission electron microscopy (TEM, JEOL 2010F STEM/TEM) were employed to examine the phase purity and microstructure. Ceramic samples for SEM were polished or polished and thermally etched at 90% of the sintering temperature for 1 h before being coated with carbon. EDX analysis was performed with an average of ten points being collected for each identified phase. An accelerating voltage of 20 kV and an effective spot size of ~2 to 3 μm was used in this procedure. This spot size was generally comparable or slightly larger than the size of secondary phase(s) and therefore EDX data from secondary phases may contain a contribution from the matrix phase. The chemical composition of the NBT perovskite phase was estimated from the analysed relative cation at% from the EDX data with the ratio of A- to B-site elements fixed as 1 : 1. TEM specimens were prepared by mechanical grinding followed by Ar-beam ion-milling.

Impedance spectroscopy was performed using a combination of an Agilent E4980A, a Solartron 1260 system (Solartron Analytical, United Kingdom) and a Solartron Modulab. Au paste (fired at 800 °C for 2 h) or Pt paste (fired at 900 °C for 2 h) electrodes were coated on both major faces of the pellets. IS data were corrected for sample geometry (thickness/area) and, additionally, high frequency data were corrected for instrumental-related inductance by performing a short circuit measurement to assess the lead resistance and associated inductance of our set-up.

Oxygen ion transport number measurements were performed on a ProboStat system (NorECs Norwegian Electro Ceramics AS,

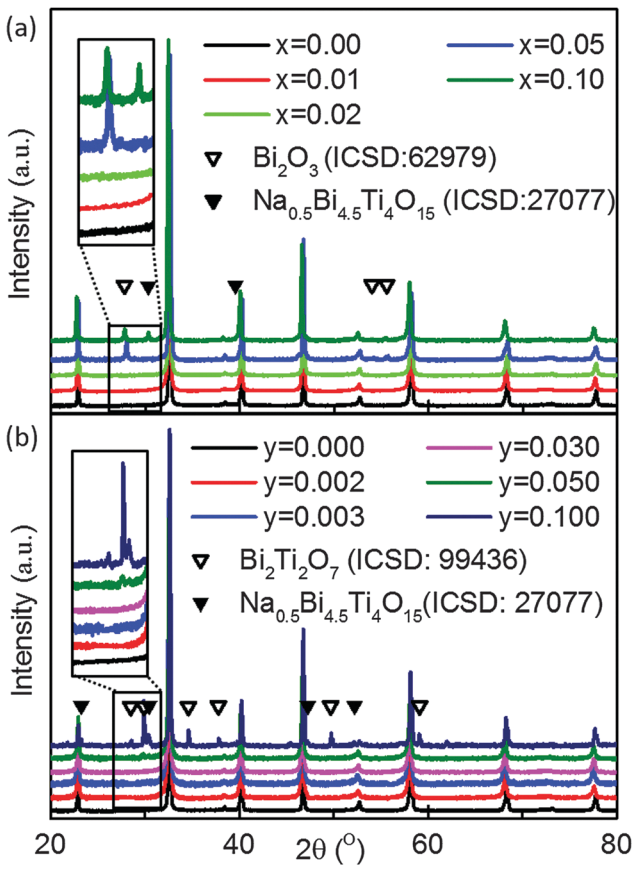

Fig. 1 Room temperature X-ray powder diffraction data for (a) $Na_{0.50}Bi_{0.50+x}TiO_{3+3x/2}$ and (b) $Na_{0.50}Bi_{0.50}Ti_{1-y}Nb_yO_{3+y/2}$ series of crushed ceramics.

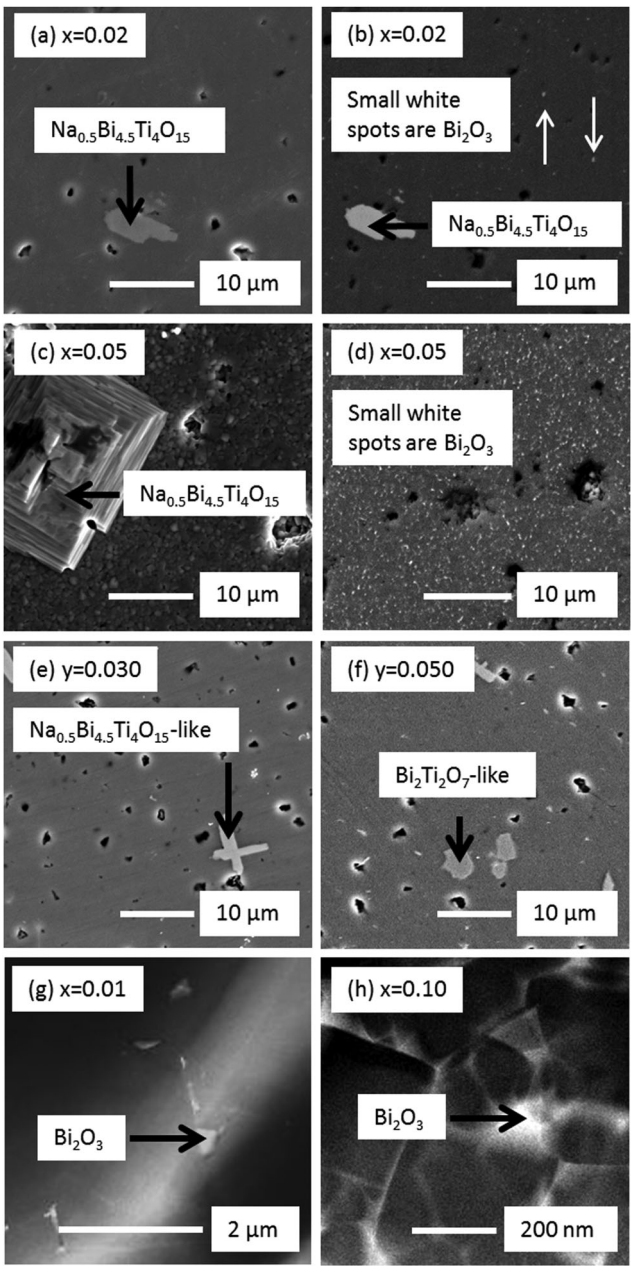

Fig. 2 SEM secondary electron images (a), (c), (e), (f) and back scattered electron images (b), (d) for selected $Na_{0.50}Bi_{0.50+x}TiO_{3+3x/2}$ and $Na_{0.50}Bi_{0.50}Ti_{1-y}Nb_yO_{3+y/2}$ ceramics. Samples were polished without thermal etching for (a), (b) and (d) to (f) and polished then thermally etched for (c). HAADF-STEM (*Z*-contrast) images for (g) $x = 0.01$ and (h) $x = 0.10$ where bright areas represent the Bi_2O_3 secondary phase.

Oslo, Norway). Dense ceramics were coated with Pt paste (fired at 900 °C for 2 h) electrodes on both major faces and sealed to one end of a YSZ tube by a commercial glass frit (KeraGlass ST K02). The voltage between the inner and outer Pt electrodes on the YSZ tube was measured to monitor the pO_2 gradient created by flowing N_2 inside the tube while keep the outside of tube in air. The generated voltage was measured by a Keithley 182 sensitive digital voltmeter (Keithley, Ohio, USA). More details can be found in Fig. S1 (ESI) in ref. 27.

Results

Laboratory XRD on crushed powders of $Na_{0.50}Bi_{0.50+x}TiO_{3+3x/2}$ sintered ceramics showed x = 0.00 to 0.02 to be phase pure whereas additional reflections were clearly observed for x = 0.05 and 0.10, Fig. 1(a). $Na_{0.5}Bi_{4.5}Ti_4O_{15}$ ($A_5B_4O_{15}$ phase) was identified by XRD as one of the secondary phases (filled triangular symbols in Fig. 1(a)) in x = 0.1 and was also confirmed in x = 0.02 and 0.05 by a combination of SEM/EDX, Fig. 2(a), (c) and Table 1. XRD data associated with the remaining additional reflections (open triangular symbols in Fig. 1(a)) were consistent with a tetragonal (β) Bi_2O_3 (space group $P\bar{4}2_1c$). However, it was not easy to detect by SEM/EDX due to its small size, as shown by the small white spots in Fig. 2(b) and (d) for x = 0.02 and 0.05, respectively. The presence of Bi_2O_3-rich pockets of secondary phase at triple point junctions between grains and along selected grain boundaries was detected in x = 0.01 by high angle annular dark field scanning transmission electron microscopy (HAADF-STEM), as shown by the bright regions in Fig. 2(g) and the elemental mapping of such a region in Fig. 3. TEM of x = 0.10 revealed a higher volume fraction of the Bi_2O_3 phase but again it was localised at triple point junctions and in the grain boundary regions, as shown by the bright regions in Fig. 2(h). EDX analysis performed on a sample of x = 0.10 using an electron probe of 1 nm did not detect the presence of any significant level of Na and/or Ti in this phase (not shown).

XRD and SEM/EDX data were consistent for $Na_{0.50}Bi_{0.50}Ti_{1-y}Nb_yO_{3+y/2}$ ceramics for $0.000 \leq y < 0.030$ and showed them to be single-phase. Although XRD data suggested y = 0.030 to be phase-pure, SEM/EDX revealed the presence of an $A_5B_4O_{15}$ secondary phase, Fig. 2(e). The average matrix composition for the perovskite phase was $Na_{0.51}Bi_{0.49}Ti_{0.97}Nb_{0.03}O_{3.00}$ and the $A_5B_4O_{15}$ phase contained Nb on the B-sublattice with a slight excess of Na for Bi on the A-sublattice with an average composition of $Na_{0.57}Bi_{4.43}Ti_{3.78}Nb_{0.22}O_{15.04}$, Table 1. The appearance of a pyrochlore-based '$Bi_2Ti_2O_7$' phase and $A_5B_4O_{15}$ as secondary phases in $y \geq 0.05$ was apparent by XRD, Fig. 1(b). SEM/EDX on y = 0.050 revealed the $A_2B_2O_7$ pyrochlore-type phase to contain Na and Bi on the A-sublattice and Ti and Nb on the B-sublattice with an average composition of $Na_{0.34}Bi_{1.59}Ti_{1.63}Nb_{0.37}O_{6.74}$ and the average matrix composition for the perovskite phase to be $Na_{0.53}Bi_{0.47}Ti_{0.95}Nb_{0.05}O_{3.00}$, Table 1 and Fig. 2(f). The average grain size in NBT is ~5 μm and is substantially reduced with increasing x or y, Fig. 4.

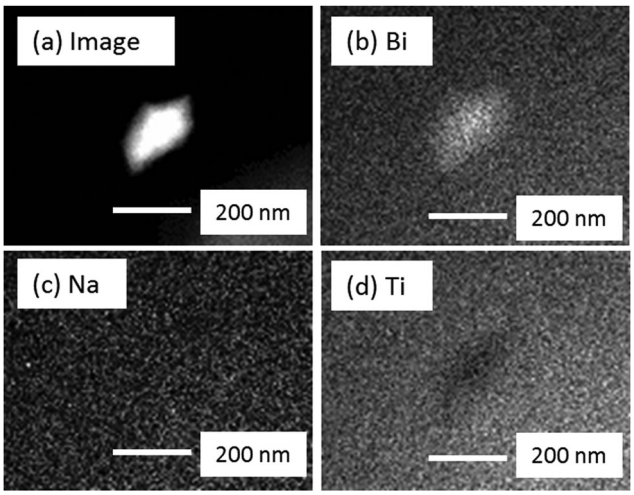

Fig. 3 (a) HAADF-STEM (Z-contrast) images for x = 0.01 and EDX mapping results of the same area for (b) Bi-mapping, (c) Na-mapping and (d) Ti-mapping.

Complex impedance plane (Z^*) plots for the x- and y-series of ceramics at ~650 °C are shown in Fig. 5. With the exception of

Table 1 Chemical composition (relative cation at%) and associated error (standard deviation) by SEM/EDX of the main and secondary phases present in x = 0.02, x = 0.05, y = 0.030 and y = 0.050 ceramics. Each value is obtained from an average of 10 analysed points. A summary of phases observed by XRD data is included for completeness. * Finely dispersed Bi_2O_3 secondary phase was detected by EDX element mapping of HAAD-STEM (Z-contrast) images, see Fig. 3 and text for details. Some totals are slightly greater than 100.0% due to rounding of values

Starting composition		Na (at%)	Bi (at%)	Ti (at%)	Nb (at%)	Observed in XRD
$Na_{0.50}Bi_{0.52}TiO_{3.030}$ (x = 0.02)	Main phase	24.3 (±0.7)	25.9 (±0.5)	49.9 (±0.3)	N/A	Yes
	$Na_{0.5}Bi_{4.5}Ti_4O_{15}$	5.5 (±0.1)	49.5 (±0.5)	45.1 (±0.4)	N/A	No
	Bi_2O_3*		Bi_2O_3			No
$Na_{0.50}Bi_{0.55}TiO_{3.075}$ (x = 0.05)	Main phase	24.4 (±0.4)	25.8 (±0.5)	49.8 (±0.5)	N/A	Yes
	$Na_{0.5}Bi_{4.5}Ti_4O_{15}$	5.2 (±0.7)	50.9 (±0.7)	44.0 (±0.6)	N/A	No
	Bi_2O_3*		Bi_2O_3			Yes
$Na_{0.50}Bi_{0.50}Ti_{0.97}Nb_{0.03}O_{3.015}$ (y = 0.030)	Main phase	25.5 (±0.3)	24.7 (±0.2)	48.0 (±0.3)	1.8 (±0.2)	Yes
	$Na_{0.5}Bi_{4.5}Ti_4O_{15}$	6.3 (±0.8)	49.1 (±0.7)	42.2 (±0.5)	2.5 (±0.2)	No
$Na_{0.50}Bi_{0.50}Ti_{0.95}Nb_{0.05}O_{3.025}$ (y = 0.050)	Main phase	26.9 (±0.4)	24.2 (±0.4)	46.3 (±0.5)	2.6 (±0.4)	Yes
	$Bi_2Ti_2O_7$	8 (±1)	40 (±2)	42 (±2)	10 (±2)	Yes
	$Na_{0.5}Bi_{4.5}Ti_4O_{15}$	Not analysed by EDX				Yes

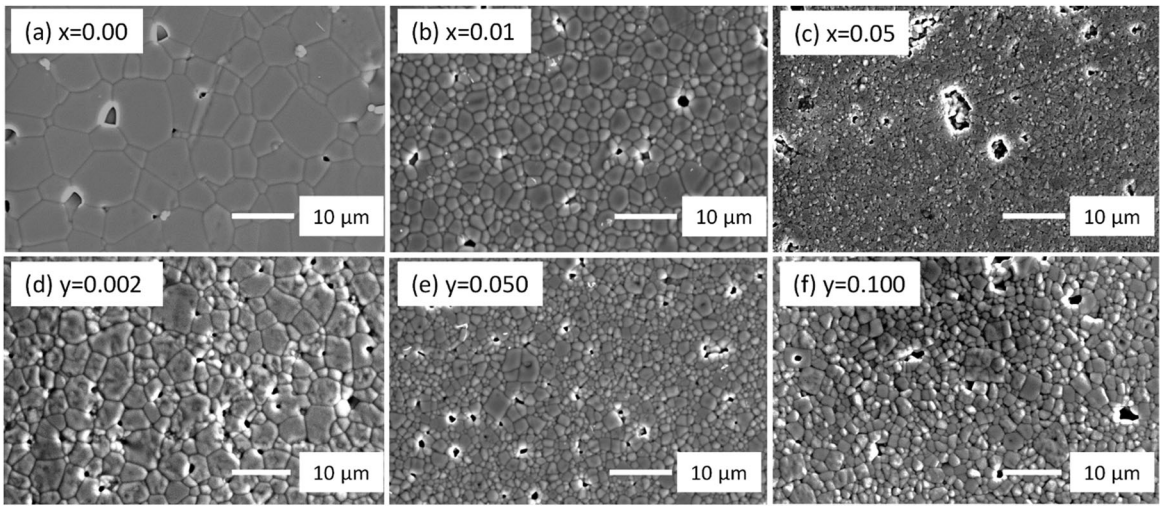

Fig. 4 SEM micrographs, (a) to (c) for selected $Na_{0.50}Bi_{0.50+x}TiO_{3+3x/2}$ and (d) to (f) for selected $Na_{0.50}Bi_{0.50}Ti_{1-y}Nb_yO_{3+y/2}$ ceramics.

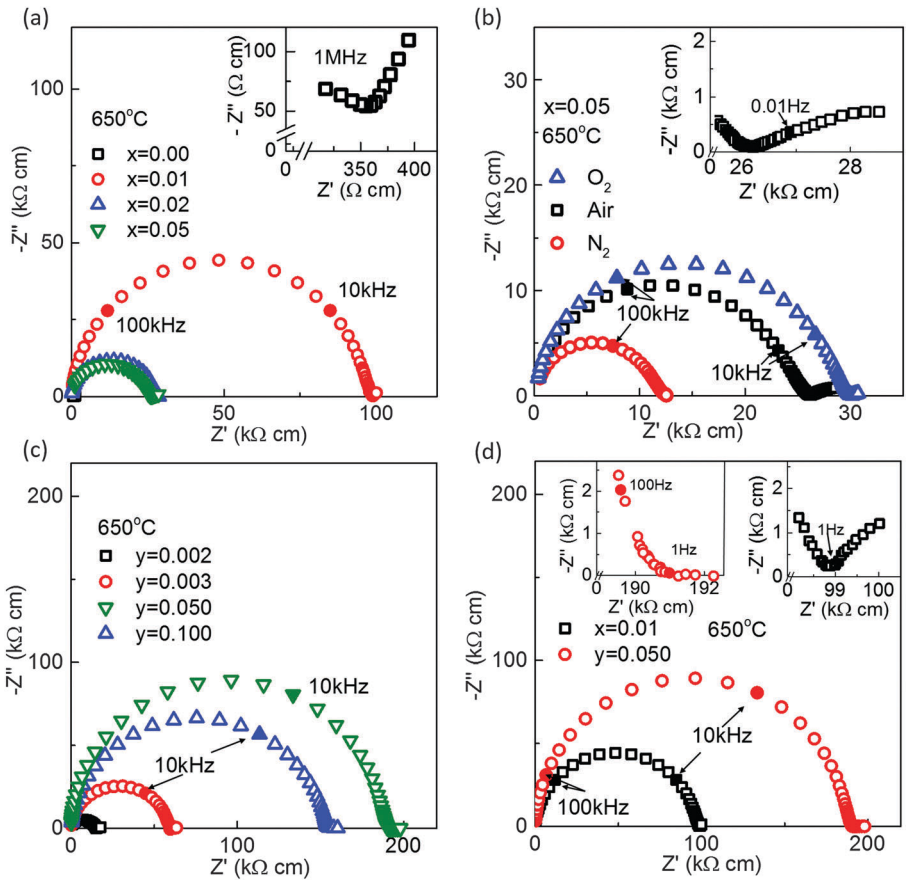

Fig. 5 Z^* plots of selected (a) $Na_{0.50}Bi_{0.50+x}TiO_{3+3x/2}$ ceramics, (b) x = 0.05, Type II ceramic, (c) selected $Na_{0.50}Bi_{0.50}Ti_{1-y}Nb_yO_{3+y/2}$ ceramics and (d) x = 0.01 and y = 0.050 Type III ceramics. All data were obtained at 650 °C.

x = 0.00, all Z^* plots were dominated by a single, large arc with the presence of a small, low frequency (<1 Hz) electrode-type response. The large and dominant arc could be modelled, to a first approximation, on a single parallel resistor–capacitor (RC) element. The associated capacitance value of the arc was consistent with a bulk (grain) response, *e.g.* C_b ~ 60–80 pF cm^{-1} which corresponds to a relative permittivity (ε_r) value of ~600 to 800 for paraelectric NBT at this high temperature. The Z^* response for x = 0.00 contained bulk, grain boundary and electrode contributions and has been reported previously.[27]

Here we show only the high frequency Z^* response of $x = 0.00$ at 650 °C, inset to Fig. 5(a), to indicate R of the bulk response (R_b) to be exceptionally low, ~360 Ω cm as compared to all other ceramics where R_b was a factor of ~50 to 500 higher, Fig. 5. In the x-series, R_b increases from ~360 Ω cm for $x = 0.00$ to ~100 kΩ cm for $x = 0.01$ before decreasing to an intermediate value of ~10–30 kΩ cm for $x \geq 0.02$, Fig. 5(a). The variation of R_b with pO_2 for $x = 0.05$ is consistent with n-type electronic behaviour, Fig. 5(b).

For the y-series, R_b increases systematically to ~15 kΩ cm for $y = 0.002$, ~55 kΩ cm for $y = 0.003$ and a maximum R_b of ~200 kΩ cm for $y = 0.050$. It then decreases to ~160 kΩ cm for $y = 0.100$ which is similar in magnitude to $x = 0.01$ and an order of magnitude larger compared to $x = 0.05$ and $y = 0.002$ and 0.003, Fig. 5(c).

The low frequency electrode response was most prominent in $x = 0.00$ (not shown, see ref. 27 for more details) but was also readily observed in x-series, inset Fig. 5(b) and (d), and $y \leq 0.003$ ceramics. The presence of a low frequency electrode arc was difficult to resolve for $y = 0.050$ and 0.100, see inset of Fig. 5(d) for data on $y = 0.050$.

t_{ion} measurements were performed on all ceramics in the range 600 to 800 °C and are listed in Table 2 together with some previously reported values.[27] The behaviour is subdivided into three categories based on the magnitude of t_{ion}. Type I, $t_{ion} \geq 0.85$, predominant oxide-ion conduction, is shown only by $x = 0.00$; Type II, $0.15 < t_{ion} < 0.85$, mixed ionic-electronic conduction is shown by $x = 0.02$, 0.05, $y = 0.002$ and 0.003; Type III, $t_{ion} \leq 0.10$, predominant electronic conduction, is shown by $x = 0.01$, $y = 0.020$, 0.050 and 0.100.

An Arrhenius plot of bulk conductivity values, $\sigma_b = 1/R_b$ over a range of temperatures and t_{ion} values at 600 °C for both series of ceramics (selected members only for reason of clarity) are shown in Fig. 6. Types I, II and III are clearly distinguished based on a combination of their high, intermediate and low σ_b and t_{ion} values. The variation of ε_r and tan δ *versus* temperature for selected ceramics reveal modest changes in $\varepsilon_{r,max}$ and T_m; however, Type I, II and III behaviour is clearly distinguished based on the magnitude of tan δ above T_m at ~325 °C, Fig. 7.

Table 2 t_{ion} values between 600 and 800 °C for selected $Na_{0.50}Bi_{0.50+x}TiO_{3+3x/2}$ and $Na_{0.50}Bi_{0.50}Ti_{1-y}Nb_yO_{3+y/2}$ ceramics. Literature values are from ref. 27

Starting composition	t_{ion} (600 °C)	t_{ion} (700 °C)	t_{ion} (800 °C)
Type I, oxygen ion conductor			
$x = 0.00$	0.93	0.93	0.85[27]
$x = -0.01$	0.92	0.92	0.90[27]
Type II, mixed ionic-electronic conductor			
$x = 0.02$	0.46	0.45	0.46
$x = 0.05$	0.62	0.64	0.65
$y = 0.002$	0.57	0.63	0.63
$y = 0.003$	0.47	0.49	0.53
Type III, insulator			
$x = 0.01$	0.07	0.07	0.10[27]
$y = 0.020$	0.05	0.06	0.06
$y = 0.050$	0.04	0.03	0.03
$y = 0.100$	0.02	0.02	0.03

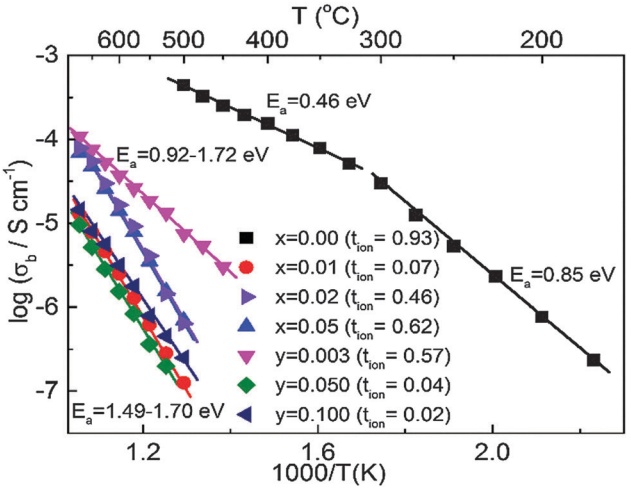

Fig. 6 Arrhenius plot of bulk conductivity, σ_b, *versus* reciprocal temperature for selected $Na_{0.50}Bi_{0.50+x}TiO_{3+3x/2}$ and $Na_{0.50}Bi_{0.50}Ti_{1-y}Nb_yO_{3+y/2}$ ceramics. Activation energy, E_a, values for σ_b and t_{ion} values at 600 °C are included.

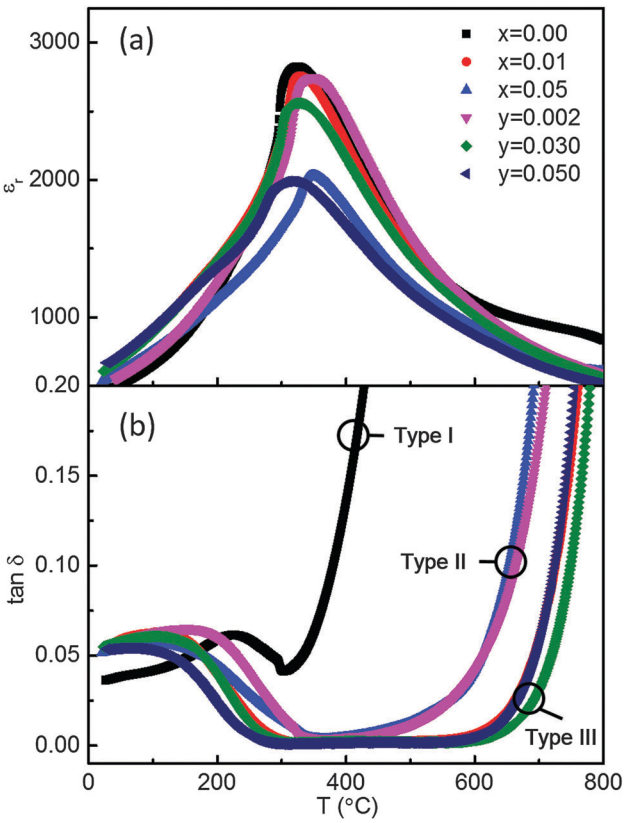

Fig. 7 (a) ε_r and (b) tan δ (both at 1 MHz) *versus* temperature for selected $Na_{0.50}Bi_{0.50+x}TiO_{3+3x/2}$ and $Na_{0.50}Bi_{0.50}Ti_{1-y}Nb_yO_{3+y/2}$ ceramics.

Discussion

The XRD and SEM results show the limits of x and y to be low, with $x < 0.01$ and $y < 0.03$, Fig. 1 and 2 but they have a dramatic effect on σ_b, tan δ and t_{ion}, Fig. 6, 7 and Table 2, respectively. In the case of simple additions of excess Bi_2O_3 (x-series), nominally stoichiometric NBT ($x = 0.00$) transforms from

Type I with high σ_b and t_{ion} (600 °C) ~ 0.93 to Type III with low σ_b and t_{ion} (600 °C) ~ 0.07 for $x = 0.01$, Fig. 6. This has very little influence on the ε_r–T profile but transforms NBT into an excellent high temperature dielectric material with $\tan\delta < 0.02$ in the range T_m to ~650 °C, Fig. 7. Further additions of Bi_2O_3 excess, *e.g.* $x \geq 0.02$, however exhibit Type II behaviour, with a significant increase in σ_b and t_{ion} (600 °C) > 0.45, Fig. 5(b), 6 and Table 2, and has a deleterious influence on the high temperature dielectric properties with $\tan\delta$ rising steeply above ~500 °C and exceeding 10% at 600 °C, Fig. 7.

At this stage it is unclear why starting compositions with $x \geq 0.02$ exhibit mixed conduction and higher conductivity but it must be linked to the presence of secondary phases, both of which are Bi-rich compared to NBT, *i.e.* $Na_{1/2}Bi_{9/2}Ti_4O_{15}$ and a Bi_2O_3 phase. Two possible explanations are; (i) a change in the Bi-content in the NBT main phase, and (ii) a space-charge model. We outline both below.

Firstly, the Bi-rich secondary phases may deplete the NBT main phase of Bi in $x > 0.01$, therefore reducing its Bi-content resulting in an increase in oxide-ion conduction. Previous studies have shown that conventional analytical methods such as EDX are unable to distinguish the low level of A-site non-stoichiometry (Na : Bi ratio) required to switch from Type I ($x = 0.00$) to III ($x = 0.01$) behaviour in NBT-based ceramics.[27] As a consequence, it is not possible to unequivocally prove a change in stoichiometry associated with the main NBT phase in the ceramics, especially due to the fine scale distribution of the Bi_2O_3-type phase in the *x*-series, Fig. 2(b) and (d). The level of *x* required to obtain Type III as opposed to Type I or II behaviour will be dependent on the ceramic processing conditions employed as they control the extent of thermodynamic equilibrium within the ceramics and this will influence the chemical potential and therefore concentration (strictly, the activity) of Bi between the three co-existing phases. In our studies, NBT powders are prepared at ~850 °C and ceramics are sintered at 1100 to 1150 °C for 2 h in air, covered in sacrificial powder of the same composition. This results in $x = 0.00$ being Type I and the requirement for a small excess of starting Bi_2O_3 ($x \sim 0.01$) to compensate for losses during processing prior to the formation of Bi-rich secondary phases to obtain Type III behaviour. *x* values are likely to be significantly different for processing conditions that don't use sacrificial powders to limit Na, Bi volatilisation and/or for higher/longer sintering periods as these factors will influence the final phase assemblage, *i.e.* composition and weight percentage of the phases present.

Secondly, enhanced ionic conductivity based on a space charge model has been observed in mixtures of two phases, based either on one ionic conductor and one insulator or mixtures of two ionic conductors.[32] For example, additions of Al_2O_3 to lithium iodide LiI led to an increase in ionic conductivity by a factor of ~50 at room temperature[33] and additions of ZrO_2 nano-powder to AgI increased ionic conductivity by more than three orders of magnitude at room temperature.[34] The interfacial space charge effect is widely considered as a driving force for the enhancement of ionic conductivity.[32] This effect may account for the enhanced oxide-ion conduction and the t_{ion} of ~0.4–0.6 in starting compositions with higher Bi-excess ($x \geq 0.02$) where NBT, Bi_2O_3-type and $Na_{0.5}Bi_{4.5}Ti_4O_{15}$-type phases coexist. The fine scale distribution of the Bi_2O_3-type phase with the NBT matrix, Fig. 2(g) and (h), combined with the fact that many Bi_2O_3-type materials exhibit high levels of oxide-ion conductivity would appear to be the most likely source of any space charge model in these ceramics. In addition, t_{ion} of these ceramics may be overestimated if the Bi_2O_3-type phase present is a good oxide-ion conductor. Further study is needed to clarify the composition and properties of this Bi_2O_3-type phase to elucidate its influence on the measured electrical properties of these ceramics and in attempts to try and distinguish between the two possible explanations outlined above.

The trend in behaviour is different for Nb-doping (*y*-series) compared to excess Bi_2O_3. Very low levels of Nb-donor doping, *e.g.* $y = 0.002$ and 0.003 transform Type I into II, and Type III behaviour is observed for $y = 0.010$ to 0.100, albeit the Nb-donor doping solid solution limit is $y < 0.030$, Fig. 1 and 2. Nb-doping is systematic and effective in 'mopping-up' and compensating for any oxygen deficiency associated with Bi_2O_3 loss during processing; t_{ion} (600 °C) decreases from 0.93 (undoped) to 0.47 for $y = 0.003$ and is <0.06 for $0.010 \leq y \leq 0.100$, Table 2. As a consequence, σ_b and $\tan\delta$ remain low for $y \geq 0.010$. All ceramics with $y \geq 0.01$ retain Type III behaviour and exhibit excellent, high temperature low dielectric loss behaviour above T_m to ~650 °C, Fig. 7(b). The ε_r–T profile for $y = 0.020$ remains similar to undoped NBT, however there is a significant decrease in $\varepsilon_{r,max}$ for $y = 0.050$, Fig. 7(a) indicating Nb-doping for Ti influences the lattice polarisability/ferroelectric domain wall motion. Again, the level of *y* required to suppress oxide-ion conduction in NBT ceramics to promote, high temperature, low dielectric low behaviour will be dependent on the ceramic processing conditions employed.

This study shows that both A-site non-stoichiometry (*via* excess Bi_2O_3) and B-site donor-doping ($Nb^{5+} + 1/2O^{2-} \rightarrow Ti^{4+}$) can be effective in fine-tuning the oxide-ion conductivity and t_{ion} in NBT. These findings are important for technical applications of NBT-based ceramics. For dielectric applications, some caution is required with the level of excess Bi_2O_3 in the starting composition as an over excess can lead to a switch from Type III to II behaviour in the presence of Bi-rich secondary phases. Excess Nb-doping therefore offers a more reliable method to retain Type III behaviour to control the level of oxygen vacancies in NBT to ensure low dielectric loss ceramics above T_m to ~650 °C. The ferroelectric/piezoelectric properties including d_{33}, depolarisation temperature and coercive field can be adjusted by tuning the concentration of oxygen vacancies. Further studies are in progress to establish the ferroelectric and piezoelectric properties of these ceramics. In addition, manufacturing of multi-layer actuators with base metal electrodes will require a balanced concentration of oxygen vacancy to increase resistance to reduction for titanium under lower pO_2 to avoid n-type semiconductivity as well as to minimise performance degradation associated with oxygen vacancies.

It is worth noting that NBT-based ceramics can be mixed conducting, albeit with a low electronic carrier concentration,

e.g. x = 0.02, 0.05, y = 0.002 and 0.003, Fig. 6 and Table 2. Although σ_b is low, the associated activation energy, E_a, for bulk conduction is high, *e.g.* >0.9 eV and tan δ remains low below ~500 °C, see Type II in Fig. 7(b), there remains a level of mobile oxygen vacancies that contribute appreciably to σ_b, as readily detected by EMF measurements, Table 2. An indication of the presence of ionic conduction in the x-series ceramics (where t_{ion} can be as low as 0.07 for Type III) can be obtained from low frequency (<1 Hz) IS measurements at elevated temperatures, as shown in the Z^* plots in the insets of Fig. 5(b) and (d) for Types II and III, respectively. In the case of y-series ceramics with Type III behaviour with $t_{ion} < 0.05$, the presence of ionic conduction was not readily observed by low frequency IS data, see inset of Z^* plot for y = 0.050 in Fig. 5(d). This highlights the value of performing EMF measurements in A-site non-stoichiometric perovskites that contain volatile species, such as Na, K, Bi and Pb, where modest levels of oxide-ion conduction (*e.g.* ~5% of σ_b) may be present.

Conclusions

We recently showed that the oxygen vacancies in the nominal starting NBT composition associated with Bi_2O_3-loss generated during sample processing can be suppressed by a small Bi-excess in the nominal starting composition ($Na_{0.50}Bi_{0.50+x}TiO_{3+3x/2}$, x = 0.01) or by Nb-donor doping ($Na_{0.50}Bi_{0.50}Ti_{1-y}Nb_yO_{3+y/2}$, $0.005 \leq y \leq 0.030$). In this work we show that further increasing the starting Bi-content ($0.02 \leq x \leq 0.10$) induces mixed ionic/electronic behaviour by reintroducing higher oxide-ion conductivity with t_{ion} ~ 0.4–0.6. For Nb-doping, mixed conduction is observed at low doping levels ($y \leq 0.003$). In contrast to increasing the Bi-excess content, increasing the Nb-donor doping level to y = 0.050, 0.100 systematically suppresses oxide-ion conductivity with $t_{ion} \leq 0.05$. The results show NBT compositions can be tuned smoothly to exhibit t_{ion} from near unity to zero. This study provides guidelines on fine-control of oxygen vacancies in NBT-based materials to tune electrical, dielectric and piezoelectric properties and to improve manufacturing practices.

Acknowledgements

The authors thank the EPSRC (EP/L017563/1) for funding.

References

1 P. Kofstad, *Nonstoichiometry, diffusion, and electrical conductivity in binary metal oxides*, Wiley-Interscience, New York, 1972.
2 D. M. Smyth, *The defect chemistry of metal oxides*, Oxford University Press, 2000.
3 A. J. Moulson and J. M. Herbert, *Electroceramics: materials, properties, applications*, John Wiley & Sons, 2003.
4 H. Kishi, Y. Mizuno and H. Chazono, *Jpn. J. Appl. Phys.*, 2003, **42**, 1–15.
5 M. Li, H. Zhang, S. N. Cook, L. Li, J. A. Kilner, I. M. Reaney and D. C. Sinclair, *Chem. Mater.*, 2015, **27**, 629–634.
6 T. Kimura, E. Fukuchi and T. Tani, *Jpn. J. Appl. Phys.*, 2005, **44**, 8055–8061.
7 F. Kulcsar, *J. Am. Ceram. Soc.*, 1959, **42**, 343–349.
8 G. H. Haertling and C. E. Land, *J. Am. Ceram. Soc.*, 1971, **54**, 1–11.
9 M. Li, L. Li, J. Zang and D. C. Sinclair, *Appl. Phys. Lett.*, 2015, **106**, 102904.
10 B. Jaffe, W. R. Cook and H. Jaffe, *Piezoelectric ceramics*, Academic Press, 1971.
11 T. Rojac, S. Drnovsek, A. Bencan, B. Malic and D. Damjanovic, *Phys. Rev. B: Condens. Matter Mater. Phys.*, 2016, **93**, 014102.
12 G. O. Jones and P. A. Thomas, *Acta Crystallogr., Sect. B: Struct. Sci.*, 2002, **58**, 168–178.
13 J. A. Zvirgzds, P. P. Kapostin, J. V. Zvirgzde and T. V. Kruzina, *Ferroelectrics*, 1982, **40**, 75–77.
14 E. Aksel, J. S. Forrester, B. Kowalski, J. L. Jones and P. A. Thomas, *Appl. Phys. Lett.*, 2011, **99**, 222901.
15 I. P. Pronin, P. P. Syrnikov, V. A. Isupov, V. M. Egorov and N. V. Zaitseva, *Ferroelectrics*, 1980, **25**, 395–397.
16 S. B. Vakhrushev, V. A. Isupov, B. E. Kvyatkovsky, N. M. Okuneva, I. P. Pronin, G. A. Smolensky and P. P. Syrnikov, *Ferroelectrics*, 1985, **63**, 153–160.
17 J. Suchanicz, K. Roleder, A. Kania and J. Hańaderek, *Ferroelectrics*, 1988, **77**, 107–110.
18 J. Suchanicz and W. S. Ptak, *Ferroelectr., Lett. Sect.*, 1990, **12**, 71–78.
19 G. O. Jones, J. Kreisel, V. Jennings, M. A. Geday, P. A. Thomas and A. M. Glazer, *Ferroelectrics*, 2002, **270**, 191–196.
20 J. Suchanicz and J. Kwapulinski, *Ferroelectrics*, 1995, **165**, 249–253.
21 J. Suchanicz, *Ferroelectrics*, 1995, **172**, 455–458.
22 E. Aksel, J. S. Forrester, J. C. Nino, K. Page, D. P. Shoemaker and J. L. Jones, *Phys. Rev. B: Condens. Matter Mater. Phys.*, 2013, **87**, 104113.
23 I. Levin and I. M. Reaney, *Adv. Funct. Mater.*, 2012, **22**, 3445–3452.
24 S. Gorfman and P. A. Thomas, *J. Appl. Crystallogr.*, 2010, **43**, 1409–1414.
25 E. Aksel, J. S. Forrester, J. L. Jones, P. A. Thomas, K. Page and M. R. Suchomel, *Appl. Phys. Lett.*, 2011, **98**, 13–16.
26 B. N. Rao, R. Datta, S. S. Chandrashekaran, D. K. Mishra, V. Sathe, A. Senyshyn and R. Ranjan, *Phys. Rev. B: Condens. Matter Mater. Phys.*, 2013, **88**, 224103.
27 M. Li, M. J. Pietrowski, R. A. De Souza, H. Zhang, I. M. Reaney, S. N. Cook, J. A. Kilner and D. C. Sinclair, *Nat. Mater.*, 2014, **13**, 31–35.
28 Y. Hiruma, H. Nagata and T. Takenaka, *J. Appl. Phys.*, 2009, **105**, 084112.
29 J. Petzelt, S. Kamba, J. Fabry, D. Noujni, V. Porokhonskyy, A. Pashkin, I. Franke, K. Roleder, J. Suchanicz, R. Klein, G. E. Kugel and J. Fábry, *J. Phys.: Condens. Matter*, 2004, **16**, 2719–2731.
30 J. Zang, M. Li, D. C. Sinclair, T. Frömling, W. Jo and J. Rödel, *J. Am. Ceram. Soc.*, 2014, **97**, 2825–2831.
31 V. A. Isupov, *Ferroelectrics*, 2005, **315**, 123–147.
32 J. Maier, *Prog. Solid State Chem.*, 1995, **23**, 171–263.
33 C. C. Liang, *J. Electrochem. Soc.*, 1973, **120**, 1289–1292.
34 K. Tadagana, K. Imai, M. Tatsumisago and T. Minami, *J. Electrochem. Soc.*, 2000, **147**, 4061–4064.

